JOURNAL OF SPACECRAFT AND ROCKETS
Vol. 42, No. 6, November–December 2005

Modeling of Mechanical Ablation in Thermal Protection Systems

R. Palaninathan* and S. Bindu†
Indian Institute of Technology, Madras 600 036, India

An integrated thermomechanical modeling of response of low-temperature ablative thermal protection system under thermal loading encountered by reentry vehicles is presented. Of the three thermal protection mechanisms, thermal, chemical, and mechanical ablations, only the latter is assumed to influence the recession in the presence of aerodynamic surface shear for materials with low shear strength at higher temperatures. A model for the mechanical ablation (erosion) is presented that is based on the matching point scheme. The degenerated doubly curved shell element is employed in the modeling. This enables consideration of the general type of aerodynamic loads, distributed and varying with surface and time coordinates, which differs from the earlier studies reported in the open literature. The finite element method uses polynomial approximation to represent the nonlinear through-thickness temperature profile and explicit-through-thickness integration in the computation of element matrices. This brings in computational efficiency without loss of numerical accuracy, particularly in the context of multilayered construction. No attempt is made to compute the incident heat flux and other aerodynamic loads. Numerical examples are presented for specified loads to bring out the influences of material properties and heating rates on surface recession and are based mostly on assumed material properties.

Nomenclature

$[B]$	=	strain–displacement matrix in stress modeling, temperature gradient matrix in thermal modeling
$[C]$	=	capacitance matrix
c	=	specific heat
$[D]$	=	matrix of direction cosines between local and global coordinates
$\{d\}$	=	global degrees of freedom (DOF)
$\{d_e\}$	=	element DOF
$[E]$	=	elasticity matrix in global coordinate system
E_1, E_t	=	moduli of elasticity in fiber and transverse directions respectively
$\{F\}$	=	load vector
G_{1t}	=	in-plane shear modulus of lamina
H_p	=	heat of pyrolysis
h_c	=	heat transfer coefficient due to convection
h_r	=	heat transfer coefficient due to radiation
h_t	=	wall thickness at time t
$[J]^*$	=	Jacobian inverse
$[K]$	=	conductivity matrix in thermal analysis, stiffness matrix in stress analysis
k	=	thermal conductivity
k_s	=	shear correction factor, $\frac{5}{6}$
N	=	shape functions in natural coordinates
nl, n	=	number of layers in the laminate
p	=	polynomial order
q	=	heat flux/unit area
S	=	shear strength
T	=	temperature
T_α	=	temperature of medium
$[T_\sigma]_{xyz}$	=	stress transformation matrix from x–y–z to X–Y–Z
$[T_\sigma]_{1ts}$	=	stress transformation matrix from 1–t–s to x–y–z
t	=	time, total laminate thickness
t_j	=	jth lamina thickness
u, v, w	=	components of displacements in the global directions
V	=	volume of element
$\boldsymbol{v}_{1i}, \boldsymbol{v}_{2i}, \boldsymbol{v}_{3i}$	=	unit vectors in local directions at node i, $\boldsymbol{v}_{3i}$ normal to surface
X, Y, Z	=	global coordinates
x, y, z	=	local coordinates, z normal to surface
α	=	coefficient of thermal expansion
α_i, β_i	=	rotations of $\boldsymbol{v}_{3i}$ about $\boldsymbol{v}_{2i}$ and $\boldsymbol{v}_{1i}$, respectively
ΔT	=	change in temperature
Δt	=	time step
Δ_R	=	surface recession
ε	=	emissivity
$\{\varepsilon\}$	=	strain vector in global system
$\{\varepsilon_0\}$	=	vector of thermal strains in global system
θ	=	fiber orientation angle, measured anticlockwise from x
ν_{1t}, ν_{t1}	=	major and minor Poisson ratios of a lamina
ξ, η, ζ	=	natural coordinates, ζ normal to the surface
ρ	=	density
σ	=	Stefan–Boltzmann constant
$\{\sigma\}$	=	stress vector in global system
τ	=	aerodynamic surface shear
ϕ	=	circumferential coordinate
1, t, s	=	principal material directions
{ }	=	column vector
⟨ ⟩	=	row vector
[ ]	=	rectangular/square matrix

Superscripts/Subscripts

e	=	element level
i	=	node number
k, j	=	layer number
p	=	pyrolysis
s	=	surface
T	=	transpose of a matrix
t, b	=	top, bottom
1, t, s	=	principal material directions
,	=	differentiation with respect to variable that follows it

Received 7 May 2004; revision received 10 March 2005; accepted for publication 10 March 2005.

*Professor, Department of Applied Mechanics; rpnathan@iitm.ac.in. Member AIAA.

†Research Scholar, Department of Applied Mechanics; currently Lecturer, Department of Civil Engineering, T.K.M. College of Engineering, Kollam 695 005, India; bindurajagopalan@yahoo.com.

Introduction

REENTRY space and hypersonic vehicles are subjected to intense aerodynamic heating. The design of suitable thermal

protection system (TPS) is essential for their successful operation. TPS is required to keep the excessive heat from destroying or damaging the vehicle or its contents at a minimum weight penalty. The design is based on the principle that the thermal energy transmitted from the boundary layer must be either absorbed, rejected, or expended. There are basically four mechanisms of thermal protection: 1) heat sink, 2) cooling, 3) surface insulation, and 4) ablation. The fourth type, namely, ablation, is a process by which thermal energy is expended by sacrifice of material and thereby absorbs a considerable amount of thermal energy. There are two categories of ablative materials: melting and nonmelting types. In melting type (thermoplastics), the liquid is removed immediately after formation and newer surface is exposed; hence, it is not efficient. In nonmelting category, again there are two types: high-temperature ablators (HTA) and low-temperature ablators (LTA). The examples of HTA are carbon–carbon (C–C) and carbon/silicon carbide ceramic matrix composites. Three-dimensional C–C composites are used in nose tip and leading edges. Because of their excellent strength retention with increase in temperature, the material remains in place and blocks the heat for longer duration and, subsequently, gets removed by oxidation at higher temperatures,[1,2] >1100 K. In the case of LTAs, mechanical ablation precedes chemical ablation because their strength reduction with temperature is appreciable. The thermal ablation (sublimation) is said to become appreciable above 3000 K. LTAs are made of char-forming plastics (thermosetts), which provide multiple levels of protection.[3] They are the materials suitable for thermal protection of ballistic missiles (high heating rates, shorter duration). The heating rates associated with flight regimes of a few reentry missions are said to vary in the range of 57–5700 W/cm^2 (Ref. 4).

Because the plastics possess low strength and stiffness, they are made into fiber-reinforced materials, for example, carbon/epoxy and carbon/phenolic composites, which renders them also suitable for load-bearing structural applications. In view of the highly orthotropic unidirectional properties (very high strength and stiffness along fiber direction and low in transverse direction), the fiber-reinforced composite structures are made into layered constructions, with fibers in individual layers oriented in preferred directions, obtained through the design. It is the plastic matrix that offers thermal protection, and hence, selection of suitable char-forming plastic is the concern of the designer. Materials such as phenolics, polymides, and polybenzimidazole are considered suitable from the points of view of char-forming ability and high values of heat of pyrolysis (heat absorbed due to decomposition into char and gases). Figure 1 shows a section of TPS wall made of a filament-wound layered shell, subjected to aerodynamic heating q and aerodynamic surface shear τ on the outer surface. Figure 1 shows various heat-absorbing mechanisms.[3] Because of the high surface temperature of char, a few phenomena occur: 1) There is reradiation of thermal energy from outer surface to atmosphere, per the fourth power law. At equilibrium temperature, the entire incoming energy is thrown back. 2) There is surface recession of the char due to oxidation (chemical ablation). 3) There is removal of soft char on the surface by the aerodynamic shear (mechanical ablation). The degradation of char strength with increase in temperature is responsible for this. The extent of char removal by mechanical ablation depends on the in-plane shear strength as a function of temperature and the severity of the aerodynamic surface shear.

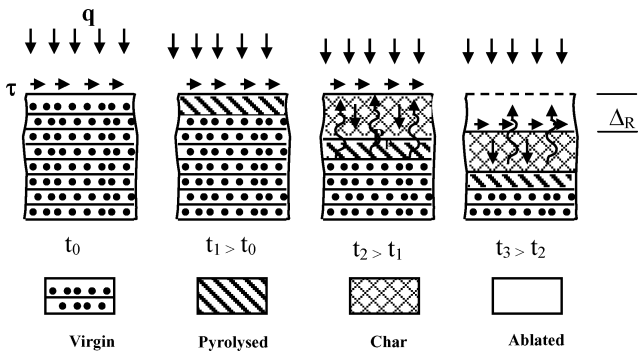

Fig. 1 Layered shell schematic, charring ablator under thermal loading.

As mentioned, low-temperature ablative TPS offers multilevel protection, encompassing multidisciplinary areas. It is difficult to account for all aspects in a single study. It is proposed to include only two effects in the present work: heat of absorption due to phase change (heat of pyrolysis) and mechanical ablation. A doubly curved layered shell element to consider arbitrarily distributed loading with polynomial approximation to represent the nonlinear through-thickness temperature distribution and explicit integration in thickness direction (assuming elements of Jacobian inverse constant through the thickness) for numerical efficiency is employed.

Previous Work

The design and development of various types of TPS have remained as topics of active research during the last 50 years. Most of the initial developments were through experimental studies, followed by analytical modeling. Even though a large body of knowledge exists, much of it is classified in nature. Heldenfels[5] has evaluated different types of construction of reentry vehicles, by comparing the heating rate with efficiencies for a total heat of 50,000 Btu/ft^2 (16.3 W/cm^2). TPS made of the charring ablator was shown to be the most suitable for higher heating rates, at which the other types become unsuitable. Matting[6] presented an analysis of charring ablation with a description of associated computing procedure. The thermal analysis is carried out with the finite difference scheme. His ablation formulation includes three elements: chemical, mechanical (erosion), and sublimation. Erosion modeling uses either an Arrhenius-type equation or a polynomial-type equation in terms of wall temperature, and the constants are obtained from material data. An illustrative example for the Apollo program has been included. Schneider et al.[7] have presented a thermal/structural analysis for shape change of graphite nose tips (solid bodies having axial symmetry) of ballistic reentry vehicles, under axisymmetric loading (zero angle of attack). Nonlinear analysis, using a finite difference technique, was employed to account for the shape change. According to Schneider et al.,[7] mechanical erosion cannot be separated from pure chemical ablation at high pressures. For lower pressures, <55 atm, chemical ablation dominates. For higher pressures, mechanical ablation combines with the latter to increase the erosion rate. The temperature range used in the ablation model is 7000–9000°R ($\approx$3890–5000 K). Chin[8] presented a formulation for three-dimensional response of ablating bodies in terms of moving coordinates. There is no mention of the mechanism of ablation used. Zien[9] presented approximate solutions for the one-dimensional ablation problem with time-dependent boundary heat flux. He dealt with melting ablation. The molten material is assumed to be removed instantaneously and completely on its formation. A mechanical–mathematical model was developed by Dimitrienko,[10] wherein he considered the ablating composites as porous multiphase media with phase transformations. His modeling considers virgin material, char after pyrolysis, and the pyrolysis gases. The rate of recession is computed based on the surface temperature. In the numerical examples, he considered composite materials, but with constant material properties. Because high temperatures are involved, this assumption introduces serious limitation on the numerical accuracy. Recently Covington et al.[11] evaluated the ablative and thermal performance of phenolic-impregnated carbon ablative (PICA), a charring material recently developed at NASA Ames Research Center, for the heat shield of Stardust Sample Return Capsule. They compared the experimental results against a fully implicit ablation and thermal computer code, FIAT, a one-dimensional code. FIAT models heat transfer though conduction and takes into account heat of pyrolysis and blowing due to pyrolysis gases. Tables 3 and 4 in Ref. 11 contain the experimental data. The maximum surface temperatures measured lie in the range of 1350–3500 K and the recession rates lie in the range 0.1–0.9 mm/s. The following observations can be made about Ref. 11. Apparently, the author have considered chemical ablation only. Had mechanical ablation been included, temperature

would not have gone to the cited levels. Also, plastic matrix composite, PICA, loses strength very fast with temperature.[12] The data do not contain information on airflow and surface shear. In these experiments, the PICA might have remained as soft material on the surface and blocked heat, before getting oxidized.

There have been a large number of studies carried out over the past few decades on the stress analyses of laminated composites, subjected to thermal loads in the form of specified temperature distributions. On the other hand, only very few have devoted attention to integrated thermomechanical analyses.[13] Dimitrienko[14] carried out an integrated analysis of a system consisting of a thermal-protective composite material for the external layer, a low-density thermoinsulative material for the middle layer, and a high-strength composite material for the internal layer. The thermal modeling is treated as linear transient problem. The cracking of outer surface char and the delamination between layers have been explained. The initiation of charring from outer surface, movement of plane of pyrolysis, and mechanism of surface recession have not been discussed.

Formulation

A degenerated doubly curved shell element has been employed for both thermal and stress modeling. This element helps to apply the arbitrarily distributed loading on the surface. Because high temperatures are involved, the material properties are functions of temperature, and hence, a nonlinear transient thermal analysis is carried out. The polynomial approximation technique is used to represent the nonlinear temperature profile through the thickness. The explicit integration scheme through-thickness is employed for computational efficiency. When an enthalpy method is used, heat of pyrolysis is accounted for. The surface erosion due to mechanical ablation is computed by a matching point scheme. The outer surface is moved inward by an amount equal to the surface erosion computed. The stress analysis is carried out before going to the next time step.

Degenerated Shell Element

The degenerated shell element, shown in Fig. 2, was derived from a three-dimensional continuum for stress analysis, using degeneration concepts.[15] The basic assumption is that linear elements straight and normal to the undeformed reference surface remain straight and inextensional even after deformation, but not necessarily normal to the deformed reference surface. This is applicable for thin and thick isotropic homogeneous shells. Numerical integration schemes in the three directions, full or selective/reduced, are employed to compute the various element matrices.

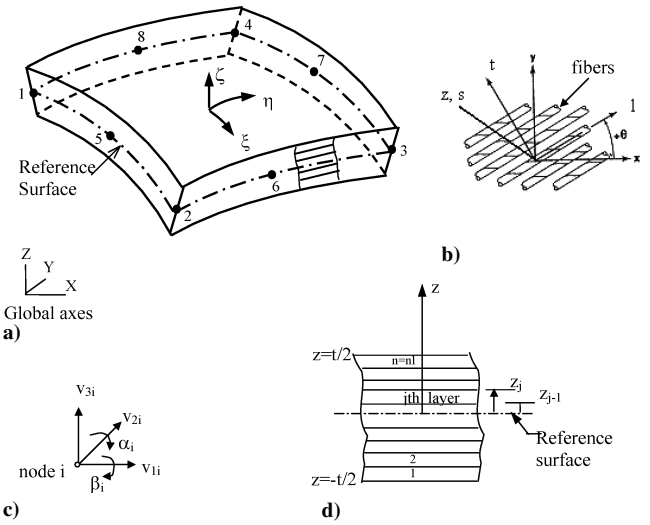

Fig. 2 Doubly curved degenerated shell element: a) eight node layered curved shell element, b) lamina with local axes system, c) unit vectors at node *i*, in local directions, and d) cross section of laminate with layer numbering and distances measured from middle/reference surface.

The coordinates of any point within the element are obtained by using

$$\begin{Bmatrix} X \\ Y \\ Z \end{Bmatrix} = \sum_{i=1}^{8} N_i(\xi,\eta) \begin{Bmatrix} X_i \\ Y_i \\ Z_i \end{Bmatrix} + \sum_{i=1}^{8} N_i(\xi,\eta)\frac{2z}{t} \begin{Bmatrix} X_i^* \\ Y_i^* \\ Z_i^* \end{Bmatrix} \tag{1}$$

where $X_i = (X_i^t + X_i^b)/2$ and $X_i^* = (X_i^t - X_i^b)/2$

The primary unknowns, namely, nodal displacements, rotations, temperatures, and temperature gradients in thickness direction, are all referred to the reference surface. The reference surface coincides with the middle surface (at $t = 0$), and its position is not altered when the outer surface starts receding due to ablation. For the stress modeling part, degrees of freedom (DOF) are the three displacement and two local rotation components at the nodes.

The displacement components at any point within the element are

$$\begin{Bmatrix} u \\ v \\ w \end{Bmatrix} = \sum_{i=1}^{8} N_i(\xi,\eta) \begin{Bmatrix} u_i \\ v_i \\ w_i \end{Bmatrix} + \sum_{i=1}^{8} N_i(\xi,\eta) z [v_{1i}, -v_{2i}] \begin{Bmatrix} \alpha_i \\ \beta_i \end{Bmatrix} \tag{2}$$

For thermal modeling, the nodal temperatures and their gradients in the thickness direction are the DOF. For the p order of approximation, the temperature at any point is written as

$$T(\xi,\eta,z) = \sum N_i(\xi,\eta) \left\langle 1 \quad z \quad \frac{z^2}{2!} \quad \frac{z^3}{3!} \quad \cdots \quad \frac{z^p}{p!} \right\rangle \begin{Bmatrix} T_i \\ T_{i,z} \\ T_{i,z^2} \\ T_{i,z^3} \\ \cdot \\ T_{i,z^p} \end{Bmatrix}$$

$$= \sum \langle \bar{N}_i \rangle \{d_e\} \tag{3}$$

Thermal Modeling (Nonlinear Transient Formulation)

The heat balance equation for an infinitesimal element is given by[13]

$$q_{X,X} + q_{Y,Y} + q_{Z,Z} = \rho c T_{,t} \tag{4}$$

The conversion of mechanical energy to thermal energy is a well-known phenomenon, usually referred to as thermal–mechanical coupling. However, in analysis of flight structures, this coupling is usually neglected[16]; hence, Eq. (4) does not contain the coupling term. The associated boundary conditions are 1) specified surface temperatures T_s; 2) specified heat flux, $q = q_0$; 3) surface convection, $q = h_c(T_s - T_\alpha)$; and 4) surface reradiation, $q = \sigma\varepsilon(T_s^4 - T_\alpha^4) = h_r(T_s - T_\alpha)$.

Using Fourier's law, the components of heat flow rate for an anisotropic medium can be written as

$$\begin{Bmatrix} q_X \\ q_Y \\ q_Z \end{Bmatrix} = -\begin{bmatrix} k_{XX} & k_{XY} & k_{XZ} \\ k_{YX} & k_{YY} & k_{YZ} \\ k_{ZX} & k_{ZY} & k_{ZZ} \end{bmatrix} \begin{Bmatrix} T_{,X} \\ T_{,Y} \\ T_{,Z} \end{Bmatrix} = -[k_{XYZ}] \begin{Bmatrix} T_{,X} \\ T_{,Y} \\ T_{,Z} \end{Bmatrix} \tag{5}$$

The material conductivity matrix in principal directions $(1, t, z)$ for a unidirectional composite (transversely isotropic material) is given as

$$[k_{1tz}] = \begin{bmatrix} k_1 & 0 & 0 \\ 0 & k_t & 0 \\ 0 & 0 & k_z \end{bmatrix}, \qquad k_z = k_t \tag{6}$$

The material conductivity matrix in local coordinate system (x, y, z) for the jth layer is obtained with suitable transformations:

$$[k_{xyz}]_j = \begin{bmatrix} k_1\cos^2\theta + k_t\sin^2\theta & (k_1 - k_t)\cos\theta\sin\theta & 0 \\ (k_1 - k_t)\cos\theta\sin\theta & k_1\sin^2\theta + k_t\cos^2\theta & 0 \\ 0 & 0 & k_t \end{bmatrix}_j \tag{7}$$

This matrix is transformed to the global directions as

$$[k_{XYZ}]_j = [D]_j^T [k_{xyz}]_j [D]_j \tag{8}$$

By following the usual finite element procedure, the derivatives of temperature with respect to the global coordinates are given by

$$\begin{Bmatrix} T_{,X} \\ T_{,Y} \\ T_{,Z} \end{Bmatrix} = [J]^*[B]\{d_e\} = [R]\{d_e\} \tag{9}$$

The variational principle is employed to obtain the governing equation. The boundary conditions are applied, and the quadratic functional associated with this equation is found. On minimization of the functional with respect to the nodal variables, we obtain the heat conduction equation in matrix form at the element level, as follows:

$$[C_e]\{d_{e,t}\} + [K_e]\{d_e\} = \{F_e\} \tag{10}$$

The computation of element matrices in Eq. (10) involves numerical integration in the three directions in each layer and then summation over layers to obtain the matrices for the whole laminate. This results in considerable increase in the computational time of various element matrices. The increase in time is directly proportional to the number of layers. Hence, this method becomes inefficient when the number of layers in the laminate is large, which is usually the case in reality. To reduce the computational time and, hence, to improve the numerical efficiency when applied to composite laminates, the scheme of explicit integration through-thickness in each layer and summation over all layers and numerical integration on the reference surface is considered very attractive.[17] The explicit integration through-thickness becomes possible due to an approximation concerning the variation of the elements of inverse of Jacobian through the thickness. These quantities may be assumed either as constant or as linearly varying through the thickness. The level of approximation would depend on the geometric parameters, particularly on the radius-to-thickness ratio. In most aerospace structures, these ratios are very high, that is, they are characterized as thin shells. In the present work, the assumption of constant Jacobian inverse across the thickness is made. The element matrices with the preceding assumption and polynomial order five have been obtained.[18] The element matrices are derived up to polynomial order five [$p = 5$ in Eq. (3)]. Once the element matrices are calculated, they are assembled to give

$$[C]\{d_{,t}\} + [K]\{d\} = \{F\} \tag{11}$$

Because the thermal properties are dependent on temperature, the resulting equations are nonlinear. The residual method has been adopted for the solution of Eq. (11). The variations of the matrices $[C]$, $[K]$, and $\{F\}$ over a time interval of Δt are assumed to be linear. The weighting function is taken as unity (subdomain method). The minimization of error over time interval Δt results in[18]

$$\lfloor \hat{K} \rfloor^* \{\Delta d\}_t + \{R\} = 0 \tag{12}$$

Solution of Eq. (12) gives the incremental values of nodal DOF at a time step.

Heat of Pyrolysis

The thermal analysis of an ablative type of TPS should include the effects of heat of pyrolysis of the material. The decomposition of thermosetts (pyrolysis) is a phase-change phenomenon. A lot of heat is consumed during this stage. This is one of the heat blocking effects of ablative TPS. In the present work, an enthalpy method is employed to consider the effect of heat of pyrolysis. Here the effect of phase change is incorporated by taking a sudden variation in the heat capacity of the material at a particular temperature, that is, the heat involved due to phase change is treated in terms of a temperature-dependent specific heat. To account for this, a new variable is introduced, namely, the enthalpy, which is the sum of the integral of the heat content with temperature and heat of pyrolysis. The effective heat capacity C^*, which accounts for the heat due to pyrolysis, is calculated[19] for each layer at Gauss points and used in the computation of capacitance matrices.

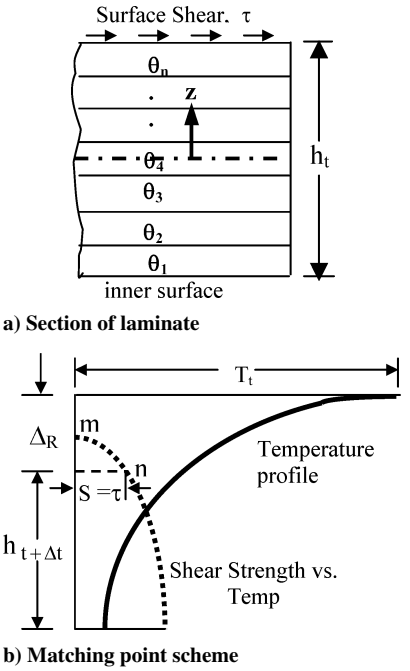

Fig. 3 Surface recession: matching of aerodynamic shear and shear strength.

Surface Recession

Figure 3a is the section of the laminate with aerodynamic surface shear τ and thickness equal to h_t at time t, where θ_i is the fiber orientation angle of ith layer. In the computation of surface recession, the variation of in-plane shear strength with temperature is required. With the temperature profile through the thickness known by the thermal analysis at any point, the variation of shear strength in thickness direction is obtained by interpolation. Figure 3b shows the variations of temperature through the thickness at any point on the middle surface, with shear strength vs temperature superposed on it. Here m is the location where shear strength becomes zero and n is the matching point where the shear strength S and the aerodynamic surface shear τ become equal. This is located by interpolation. The surface recession Δ_R is the distance from the outer surface to the matching point. The material on the outer surface, equal to the thickness of Δ_R, is removed before undergoing stress analysis and the subsequent thermal analysis.

The surface recession/boundary movement described has been incorporated in the present formulation using a degenerated layered shell element, as shown schematically in Fig. 4. Initially, the number of layers is equal to nl and the reference surface coincides with the middle surface, $z^t = t/2$, $z^b = -t/2$ (Fig. 4a). As time proceeds, the recession starts and Δ_R is less than a lamina thickness. That is, a fraction of the outer layer is removed (Fig. 4b). With time, the extent of material removal increases, resulting in loss of more layers ($n <$ nl and $z^t < t/2$, Fig. 4c). In the described scheme, note that the reference surface is not changed, that is, the distance of the inner surface from the reference surface is always equal to $-t/2$. However, the distance of the outer surface is decreasing with time. The need for maintaining the reference surface constant arises from the fact that, in the solution scheme, only the incremental nodal variables, that is, temperature and its derivatives in thickness direction at the reference surface, are calculated at each time step and added to the preexisting values. When the reference surface is maintained constant, it becomes possible to establish one-to-one correspondence on the nodal variables between the time steps.

Stress Modeling

The same degenerated doubly curved shell element shown in Fig. 2 is employed in the stress modeling also. The matrix of thermal strains in global coordinate system for the jth layer is obtained with suitable transformations, first from the principal material directions

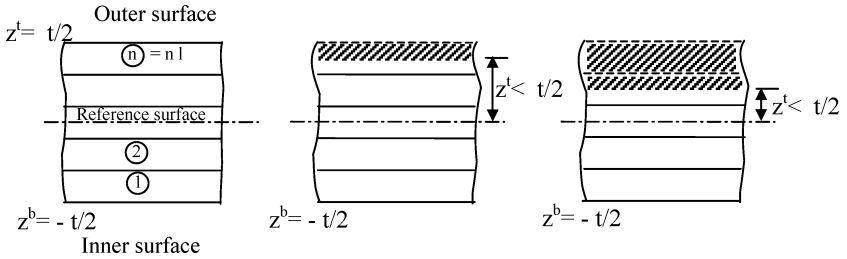

a) Before recession, $n = nl$ **b) Recession starts, $n = nl$** **c) Substantial recession, $n < nl$**

Fig. 4 Finite element modeling of surface recession.

to the element local directions (x, y, z) and second from local to global directions (X, Y, Z) as follows:

$$\begin{Bmatrix} \varepsilon_{0X} \\ \varepsilon_{0Y} \\ \varepsilon_{0Z} \\ \gamma_{0YZ} \\ \gamma_{0ZX} \\ \gamma_{0XY} \end{Bmatrix} = [T_\varepsilon]_{xyz}[T_\varepsilon]_{1ts} \begin{Bmatrix} \alpha_1 \\ \alpha_t \\ 0 \\ 0 \\ 0 \\ 0 \end{Bmatrix} \Delta T \tag{13}$$

After applying the degenerated shell assumptions,[15] the elasticity matrix in the principal material directions (transversely isotropic material) can be written as

$$[E_{1ts}]_j =$$

$$\begin{bmatrix} \dfrac{E_1}{1-\nu_{1t}\nu_{t1}} & \dfrac{E_t\nu_{1t}}{1-\nu_{1t}\nu_{t1}} & 0 & 0 & 0 & 0 \\ \dfrac{E_t\nu_{1t}}{1-\nu_{1t}\nu_{t1}} & \dfrac{E_t}{1-\nu_{1t}\nu_{t1}} & 0 & 0 & 0 & 0 \\ 0 & 0 & 0 & 0 & 0 & 0 \\ 0 & 0 & 0 & \dfrac{k_s E_t}{2(1+\nu_{st})} & 0 & 0 \\ 0 & 0 & 0 & 0 & k_s G_{1t} & 0 \\ 0 & 0 & 0 & 0 & 0 & k_s G_{1t} \end{bmatrix} \tag{14}$$

The elasticity matrix $[E]_j$, for the jth layer, in the global coordinate system is obtained by two-stage transformations,[20] first from the material directions $(1\text{–}t\text{–}s)$ to local directions $(x\text{–}y\text{–}z)$ and second from local to global directions $(X\text{–}Y\text{–}Z)$ (Fig. 2) as

$$[E]_j = [T_\sigma]_{xyz}[T_\sigma]_{1ts}[E_{1ts}]_j[T_\sigma]^T_{1ts}[T_\sigma]^T_{xyz} \tag{15}$$

To make the computations efficient, the method of explicit integration across the thickness was suggested,[17] as mentioned earlier, under thermal modeling. Based on these assumptions, the strain–displacement matrix $[B]$ is expressed in two parts as

$$[B] = [B_1] + z[B_2] \tag{16}$$

$[B_i]$ are independent of the thickness coordinate. This makes the computation of element stiffness matrix much simpler (model IV of Premakumar and Palaninathan[21]). Explicit integration is carried out across the thickness and numerical integration on the reference surface.[18] The element matrices are assembled to obtain a global set of equations and solved for displacements. When the solution vector of displacements is used, the strains for the jth layer are calculated as

$$\{\varepsilon\}_j = [[B_1] + z[B_2]]\{d_e\} \tag{17}$$

The stresses in the global frame are obtained from

$$\{\sigma\}_j = [E]_j\{\{\varepsilon\}_j - \{\varepsilon_0\}_j\} \tag{18}$$

The stresses in local and material directions are then obtained by appropriate transformations.

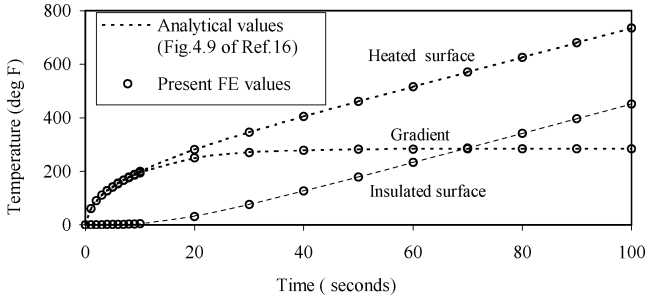

Fig. 5 Transient thermal response of thin graphite/epoxy plate.

Validation Checks

The formulation for the ablative TPS presented in the earlier sections was subjected to validation checks using simple thermal and structural problems for which results are available in literature.[16,22] The latest reference on the topic of LTA ablation is that of Covington et al.[11] However, it does not address the mechanical ablation model, and hence, validation checks on this aspect are not possible as of yet.

Transient Thermal Response of a Suddenly Heated Thin Plate

A thin plate of graphite/epoxy composite material (not a fiber composite) is subjected to a uniformly distributed heat flux of 0.1 Btu/in.$^2 \cdot$s on one surface and the other surface is insulated. The thickness of the plate is 0.125 in. The thermal conductivity of material is $2.2e{-}05$ Btu/in. $\cdot$ s $\cdot$ °F and thermal diffusivity is $1.5e{-}04$ in.^{2}/s. An analytical solution for this is available.[16] The variations of temperature with time are computed for the heated and the insulated surfaces and are shown in Fig. 5. The gradient is calculated as the difference in temperature between the heated and the insulated surfaces. The results show good agreement between the present values and the analytical solution.

Isotropic Shell Subjected to Linearly Varying Temperature Profile

The mean radius of the cylindrical shell is 100 mm and thickness is 1 mm, $E = 31.0e{+}06$ MPa, $\nu = 0.3$, and $\alpha = 2.15e{-}06$/K. Reference temperature is 0 K. The shell is subjected to a linearly varying temperature profile with a temperature of $+150$ K on the outer surface and -150 K on the inner surface. Because of symmetry one-eighth of the cylinder is analyzed with 4×4 mesh. The edges are free to expand. The maximum stress in the hoop and axial directions, away from the edges are given by[22] $\sigma = +, -[\alpha(T_2 - T_1)E/2(1-\nu)]$, where T_2 is the outer surface temperature and T_1 is the inner surface temperature and the first sign $(+)$ refers to the outer surface.

The comparison of results of the present finite element analysis with the exact solution,[22] is given in Table 1. Very good agreement is seen to exist between the two values.

Numerical Examples

In this section, we present a few numerical examples that are considered representative for TPS of reentry vehicles. A layered cylindrical shell of 500-mm inner radius and 20-mm wall thickness

Table 1 Stresses in isotropic cylindrical shell subjected to linearly varying temperature profile through the thickness

Stress, MPa	Present	Timoshenko and Krieger[22]
Hoop		
Outer surface	−14,282.6	−14,282.14
Inner surface	−14,281.3	−14,282.14
Axial		
Outer surface	−14,280.0	−14,282.14
Inner surface	−14,282.6	−14,282.14

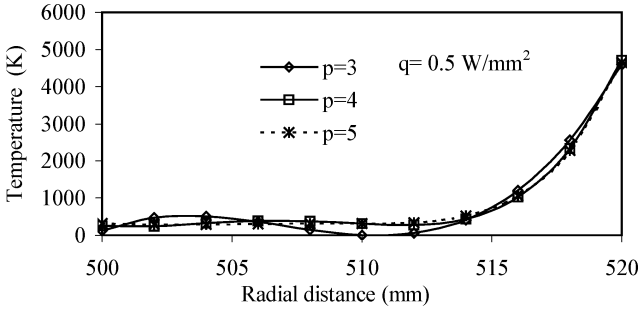

Fig. 6 Temperature profiles for different polynomial orders at $t = 30$ s.

with 20 layers of filament wound composite is considered. The material properties are that of nylon/phenolic,[23] dependent on temperature, unless stated otherwise. Values of a few properties at room temperature are $k_1 = 0.337e{-}3$, $k_t = 0.337e{-}3$ W/mm · K, $\rho = 0.1201e{-}5$ kg/mm^3, $c = 1.28e{+}3$ J/kg · K, $H_p = 0$, $E_1 = 1.30e{+}5$, and $E_t = 2.02e{+}4$ N/mm^2. Numerical studies are presented for 1) aerodynamic heating uniformly distributed on the surface and 2) nonuniformly distributed. The influence of various parameters, such as polynomial order, thermal conductivity, heat of pyrolysis, reradiation loss, and surface shear on temperature profiles and surface erosion rates has been studied. The general requirements of finite element formulation, namely, convergence checks and computational efficiency of the explicit through-thickness schemes with regard to thermal and stress modeling were verified in earlier studies.[21,24] The numerical examples presented here are obtained using a Pentium IV Personal computer with 2.4-GHz speed and 512-MB RAM. The clock time for solving a specific problem was about 45 min, with time step of 0.1 s for 50-s duration of solution.

Heat Flux Uniformly Distributed on the Surface

Effect of Polynomial Order

In the thermal modeling, a polynomial approximation is employed to represent the nonlinear through-thickness temperature distribution. The selection of appropriate order p for approximation is necessary. The analysis of cylindrical shell, subjected to a heating rate of 0.5 W/mm^2 on outer surface and initial temperature at 300 K, is carried out for polynomial orders $p = 3$–5, neglecting the reradiation loss. Figure 6 shows the through-thickness temperature profiles for $t = 30$ s. The outer surface temperature rises very fast, and the heating takes place within outer one-third part. The temperature in the inner two-thirds part is almost equal to 300 K. For $p = 3$, there is considerable variation (oscillation) in the temperature distribution in inner-half and for $p = 5$, it disappears, and the temperature becomes almost constant. Figure 7 shows the through-thickness temperature profiles for $p = 5$ at different time levels. The surface temperature reaches a value of 5700 K at $t = 50$ s. The surface reaching such a high temperature is only a hypothetical case. However, earlier researchers have also predicted surface temperature of this order.[7] The temperature in the inner-half remains constant, equal to the initial value of 300 K. The polynomial order $p = 5$ seems to be the optimum and, hence, used in the examples that follow.

Effect of Reradiation Loss

The temperature profiles are obtained with and without reradiation loss and are shown in Fig. 8. When this effect is neglected, the surface temperature goes up to 5700 K. When this is included, the surface temperature rises up to only 1600 K.

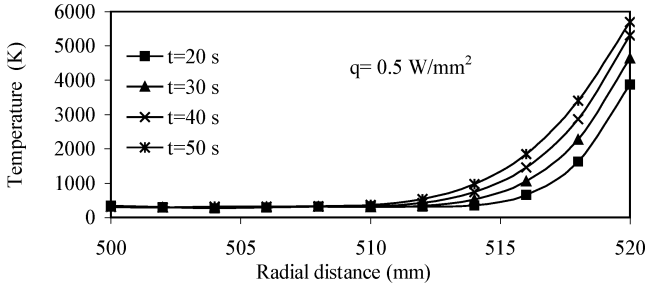

Fig. 7 Temperature profile across the thickness for $p = 5$.

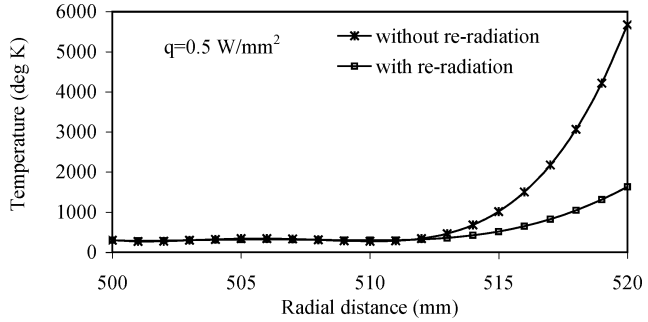

Fig. 8 Through-thickness temperature profile, $t = 50$ s, with and without reradiation.

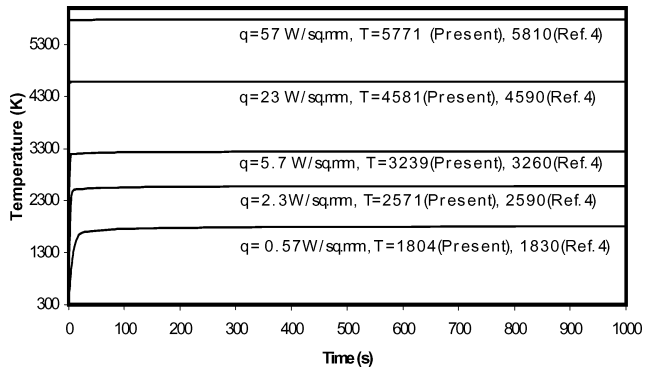

Fig. 9 Radiation equilibrium temperatures for different heating rates (Ref. 4).

Equilibrium Temperature

With the reradiation effect included, the surface temperature increases with time initially and then reaches a steady value (equilibrium temperature), the level of which depends on the heating rate. To investigate this aspect, thermal analyses are carried out for different heating rates, ranging from 0.57 to 57 W/mm^2. The surface temperature vs time are shown in Fig. 9. The equilibrium temperature for the lowest heating rate (0.57 W/mm^2) is 1700 K. In the case of the space shuttle, the maximum surface temperature encountered is of this order,[16] wherein ceramic tiles are used for TPS. For the highest heating rate considered (57 W/mm^2), the equilibrium temperature goes up to about 5600 K. The equilibrium temperatures shown compare reasonably well with the literature.[4]

Surface Recession

The model for surface recession has been presented earlier (Fig. 4). The controlling parameters are temperature of pyrolysis T_p, heat of pyrolysis H_p, aerodynamic surface shear τ, and in-plane shear strength S of the TPS material as function of temperature. Figure 10 shows typical material shear strength vs temperature of a composite material.[12] Numerical examples are presented here for

assumed values of $T_p = 500$ K, $\tau = 5$ MPa, and $H_p = 0$. The temperature profile and hoop stress across the thickness are presented in Fig. 11 for the two cases, with and without surface recession with uniformly distributed surface heating, $q = 0.5$ W/mm^2. Note that when surface recession is accounted for, the surface temperature only rises up to about 650 K, as against 5000 K when recession is not accounted for. The hoop stress reduces to 150 MPa (compressive) from 1000 MPa (compressive) between the two cases. However, the outer boundary has moved by about 15 mm during time interval of 40 s. About 75% of the material has been sacrificed. This ablation process is presented schematically in Fig. 12 at four time levels. The horizontal lines indicate the layers in the laminate. Initially the total number of layers is 20, and it reduces to 16 at $t = 10$ s, to 12 at $t = 20$ s, and to 5 at $t = 40$ s. The char thickness remains constant, about 1 mm at all time steps. Δ_R is the ablation/recession depth. Because the heating is assumed uniformly distributed, Δ_R is equal at all points on the surface of cylindrical shell. Also, note that the reference surface for the shell element formulation initially coincides with the middle surface. As described in the surface recession modeling (Fig. 4), this reference surface is maintained at the same location, even though the layers are removed by ablation at higher time levels. There is no need move this surface. Having unequal thickness on either side of reference surface does not affect the performance of the shell element. However, it shall increase the severity of the bending–stretching coupling in the structural behavior, which is not unusual in laminated composite shell theory. With reference to Figs. 11 and 12, three more observations may be made regarding the design for structural adequacy. One, the number of virgin layers remaining at the end of the mission should be adequate to provide structural design requirements such as impact and buckling strengths and to withstand the aerodynamic surface pressure acting on the external surface. In other words, the design of wall thickness of a TPS needs to be based on both ablative and structural requirements. This paper does not address impact and buckling strength aspects. Two, the temperature level in the virgin layers is almost at the initial level (300 K), and hence, the material properties at room temperature can be used in the structural design checks. Three, because char thickness is small (about 1 mm), the heat blocking effect of escaping pyrolysis gases may be neglected.

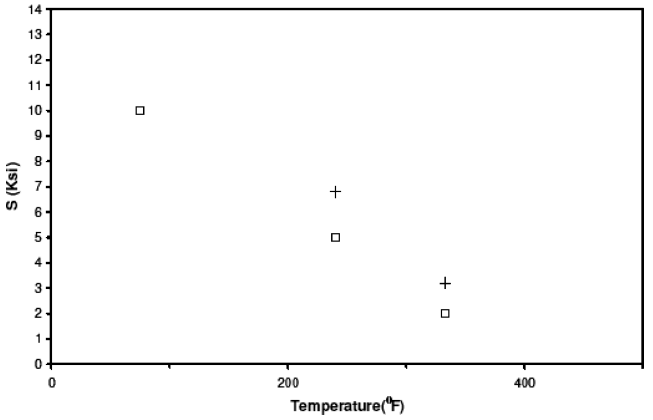

Fig. 10 Shear strength vs temperature for graphite/epoxy[12]: □, solid tab and +, flexible tab.

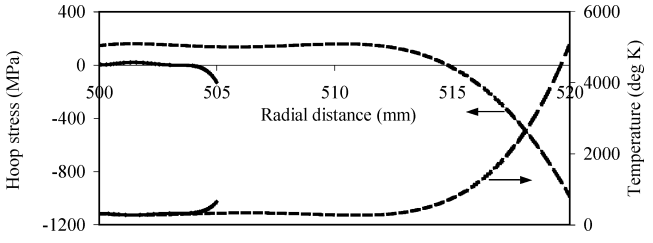

Fig. 11 Variation of temperature and hoop stress across the thickness, with and without surface recession at $t = 40$ s, heating rate $q = 0.5$ W/mm^2: - - - -, without surface recession and ——, with surface recession.

Solution for this thermomechanical problem is obtained in small increments of time Δt, and extent of surface recession Δ_R is computed at each time step. The recession rate is obtained as $\Delta_R/\Delta t$. The recession rates for three heating rates, $q = 0.5$, 1.0, and 2.0 W/mm^2, are shown in Fig. 13a. It may be seen that initially the recession rate is zero (warming up period, which is less than 1 s and depends on the heating rate), suddenly shoots up to a peak value of 3 mm/s for $q = 2.0$ W/mm^2 (transient condition), and subsequently decreases and then stabilizes at a steady value of about 0.75 mm/s. The corresponding values for $q = 0.5$ W/mm^2 are 0.75 and 0.35 mm/s. Figure 13b shows the effect of aerodynamic surface shear τ on the recession rate. There is an increase of about 0.1 mm/s when the shear stress τ is increased from 0 to 30 MPa.

The influence of heat of pyrolysis on the surface recession is studied by taking three values, $H_p = 0, 10^5$, and 10^6 J/kg. The first two are hypothetical values, and the third is close to that of nylon/phenolic.[23] Figure 13c shows the variations of surface recession with time. The peak recession rate is about 0.75 mm/s and the steady value is about 0.35 mm/s, for $H_p = 0$. The recession rate reduces considerably when H_p is increased. The peak value is about 0.3 mm/s and the steady value is about 0.2 mm/s for $H_p = 10^6$ J/kg. Also note that higher value of heat of pyrolysis delays the onset of surface recession.

Varying Heat Flux Applied over the Surface

The strength of the present formulation lies in its capability to analyze cases of varying heat flux, nonuniformly distributed on the

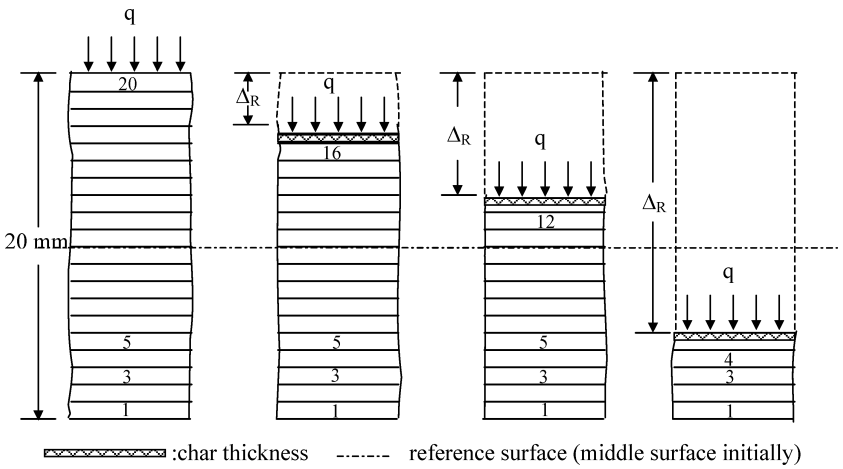

a) $\Delta_R = 0$, $t = 0$ s b) $\Delta_R = 3.6$ mm, $t = 10$ s c) $\Delta_R = 7.3$ mm, $t = 20$ s d) $\Delta_R = 15$ mm, $t = 40$ s

Fig. 12 Circular cylindrical shell, uniform surface heating ($q = 0.5$ W/mm^2); section of laminate across thickness at different times.

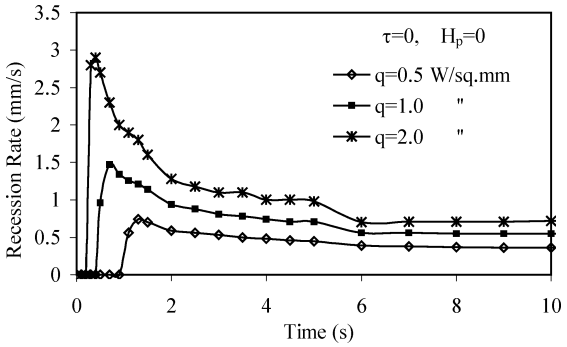

Fig. 13a Recession rate vs time effect of heating rates.

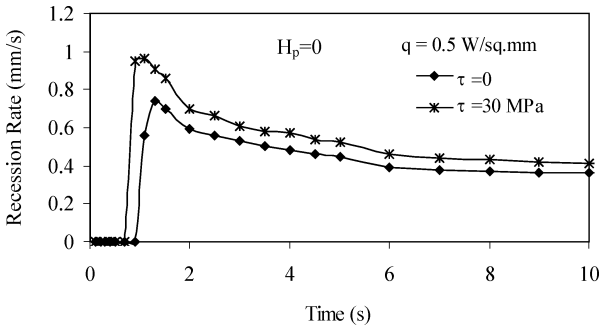

Fig. 13b Recession rate vs time effect of aerodynamic shear.

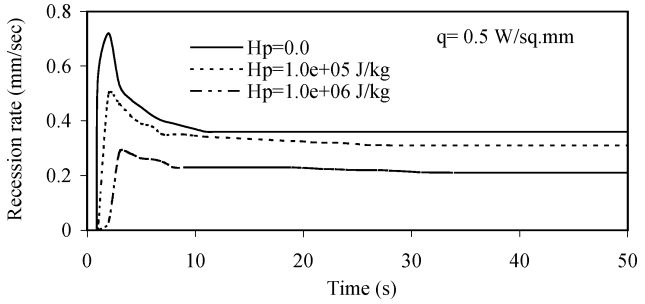

Fig. 13c Recession rate effect of heat of pyrolysis.

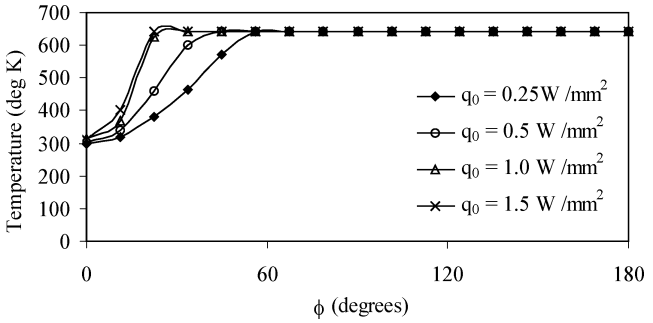

Fig. 14 Outer surface temperature vs angular location under circumferentially varying heat flux, $q = q_0(1-\cos\phi)/2$, at time $t = 40$ s.

surface and varying with time and that, in this respect, it differs from the earlier formulations. One numerical example is presented here to show this effect. The geometric and material data are same as that of the examples presented earlier, except that the wall thickness has been increased to 40 mm. The intensity of surface heating is assumed to vary in the circumferential direction as $q = q_0\,(1 - \cos\phi)/2$ and remain constant in the axial direction of the cylindrical shell. Numerical values are obtained with $q_0 = 0.25, 0.5, 1.0$, and $1.5\ \text{W/mm}^2$.

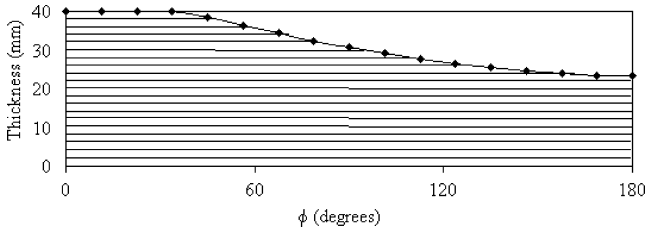

a) $q_0 = 0.5\ \text{W/mm}^2$

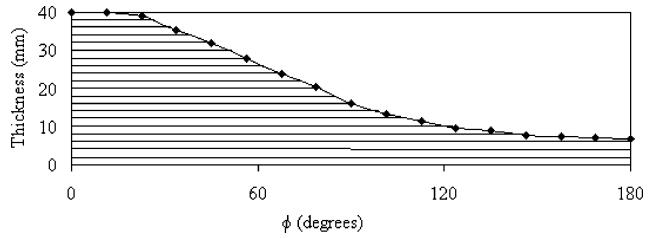

b) $q_0 = 1.5\ \text{W/mm}^2$

Fig. 15 Laminate thickness vs angular location under circumferentially varying heat flux, $q = q_0(1-\cos\phi)/2$, at time $t = 40$ s, $\tau = 5$ MPa, $H_p = 0$.

Figure 14 shows the variation of the surface temperature with ϕ at $t = 40$ s. The temperature remains almost constant at $\phi = 0$, indicating that the heat flow is almost unidirectional. It varies with ϕ initially, up to about 60 deg, depending on the heat flux intensity, and then it remains constant at about 650 K for $\phi > 60$ deg. The surface temperature has been restricted to this level, because of early removal surface material by mechanical ablation. Even though the temperature remains constant over a larger region, the recession has taken place and the depth varies with ϕ and reaches a maximum at $\phi = 180$ deg. Its variation does not follow the loading pattern, $q = q_0(1 - \cos\phi)/2$ (Fig. 15).

Summary

The present modeling is based on the finite element method, the most powerful numerical procedure, and hence, the analyses of ablative TPS can be carried out close to reality for uniformly or nonuniformly distributed and time-varying loads and also taking the variations of material properties with temperatures into account. This mechanical ablation model, presented in the open literature probably for the first time, needs to be verified against experimental data. Based on the numerical examples presented, a few concluding remarks are made. In the representation of nonlinear through-thickness temperature, fifth-order polynomial approximation is considered necessary for problems of this nature. The reradiation effect needs to be accounted for in the formulation. This is a major heat blocking (heat throwing) mechanism in hyperthermal environments. The heat of pyrolysis has a significant influence in absorbing the incoming heat into the system. It signifies the thermal energy consumed during decomposition of char-forming plastics. This property can be a yardstick in the evaluation of various materials for LTAs. The aerodynamic surface shear is seen to influence the recession marginally. On the other hand, the rate of degradation of shear strength with temperature has considerable influence. In the case of a nonuniformly distributed heat flux on the surface, even though the heat conduction is primarily one dimensional (flow normal to the surface), the surface recession does not follow the pattern of heating and, hence, the use of doubly curved shell elements assumes importance. The present paper does not include the effects of heat blockage due to chemical and thermal ablations; however, they can be included, at later stage, if desired, to improve the accuracy.

References

[1]Han, J. C., He, X. D., and Du, S. Y., "Oxidation and Ablation of 3D Carbon–Carbon Composite up to 3000°C," *Carbon*, Vol. 33, No. 4, 1995, pp. 473–478.

[2]Hatta, H., Takuya, A., Yasuo, K., and Toshio, Y., "High Temperature Oxidation Behaviour of SiC Coated Carbon Fibre Reinforced Carbon Matrix Composites," *Composites Part A*, Vol. 30, No. 4, 1999, pp. 515–520.

[3]D'Alelio, G. F., and Parker, J. A., *Ablative Plastics*, Marcel Dekker, New York, 1971, Chap. 1.

[4]Lee, S. M., *International Encyclopedia of Composites*, Vol. 1, VCH, New York, 1990, p. 428.

[5]Heldenfels, R. R., "Structures for Manned Entry Vehicles," *Proceedings of Conference on Aerodynamically Heated Structures*, edited by P. E. Glaser, Prentice–Hall, 1962, pp. 197–218.

[6]Matting, F. W., "Analysis of Charring Ablation with Description of Associated Computing Program," NASA TN D-6085, Nov. 1970.

[7]Schneider, P. J., Teter, R. D., Coleman, W. D., and Heath, R. M., "Design of Graphite Nose Tips for Ballistic Re-Entry," *Journal of Spacecraft and Rockets*, Vol. 10, 1973, pp. 592–598.

[8]Chin, J. H., "Shape Change and Conduction for Nose Tips at Angle of Attack," *AIAA Journal*, Vol. 13, No. 5, 1975, pp. 599–604.

[9]Zien, T. F., "Integral Solutions of Ablation Problems with Time-Dependent Heat Flux," *AIAA Journal*, Vol. 16, No. 12, 1978, pp. 1287–1295.

[10]Dimitrienko, Y. I., "Thermal Stresses and Heat-Mass Transfer in Ablating Composite Materials," *International Journal of Heat and Mass Transfer*, Vol. 38, 1995, pp. 139–146.

[11]Covington, M. A., Heinemann, J. M., Goldstein, H. E., Chen, Y. K., Terrazas-Salinas, I., Balboni, J. A., Olejniczak, J., and Martinez, E. R., "Performance of Low Density Ablative Heat Shield Material," AIAA Paper 2004-2273, June–July 2004.

[12]Sun, C. T., and Yoon, K. J., "Mechanical Properties of Graphite/Epoxy Composites at Various Temperatures," School of Aeronautics and Astronautics, Rept. NTIS AD A 199 311, Purdue Univ., Lafayette, IN, Jan. 1988.

[13]Dechaumphai, P., and Thornton, E. A., "Improved Finite Element Methodology for Integrated Thermal Structural Analysis," NASA CR 3635, Nov. 1982.

[14]Dimitrienko, Y. I., "Thermal Stresses in Ablative Composite Thin-Walled Structures Under Intensive Heat Flows," *International Journal of Engineering Science*, Vol. 35, 1997, pp. 15–31.

[15]Ahmad, S., Irons, B. M., and Zienkiewicz, O. C., "Analysis of Thick and Thin Shell Structures by Curved Finite Elements," *International Journal for Numerical Methods in Engineering*, Vol. 2, 1970, pp. 419–451.

[16]Thornton, E. A., "Thermal Structures: Four Decades of Progress," *Journal of Aircraft*, Vol. 29, No. 3, 1992, pp. 485–498.

[17]Vlachoutsis, S., "Explicit Integration for Three-Dimensional Degenerated Shell Finite Elements," *International Journal for Numerical Methods in Engineering*, Vol. 29, No. 4, 1990, pp. 861–880.

[18]Bindu, S., "Thermo-Mechanical Modeling of Thermal Protection System," Ph.D. Dissertation, Dept. of Applied Mechanics, Indian Inst. of Technology, Madras, India, Feb. 2004.

[19]Morgan, K., Lewis, R. W., and Zienkiewicz, O. C., "An Improved Algorithm for Heat Conduction Problems with Phase Change," *International Journal for Numerical Methods in Engineering*, Vol. 12, No. 7, 1978, pp. 1191–1195.

[20]Lekhnitskii, S. G., *Theory of Elasticity of an Anisotropic Body*, MIR, Moscow, 1981, pp. 39–50.

[21]Premakumar, W. P., and Palaninathan, R., "Finite Element Analysis of Laminated Shells with Exact Through-Thickness Integration," *Computers and Structures*, Vol. 63, No. 1, 1997, pp. 173–184.

[22]Timoshenko, S., and Woinowsky-Krieger, S., *Theory of Plates and Shells*, McGraw–Hill, New York, 1959, Chap. 2.

[23]Witte, W. G., "Analysis of the Thermal Response of High-Density Phenolic-Nylon on a Spacecraft Launched by the Pacemaker Vehicle System," NASA TN D-6293, May 1971.

[24]Kennedy, P. J. P., and Palaninathan, R., "p-Approximation Finite Elements for Heat Conduction in Laminated Shells with Exact Through Thickness Integration," *Journal of the Aeronautical Society of India*, Vol. 47, No. 4, 1995, pp. 246–256.

T. Lin
Associate Editor